

## Spare Theory for the Detection of Brain Tumor using Multimodal Medical Image Fusion

S. L. Jany Shabu<sup>1</sup>, C. Jayakumar<sup>2</sup>, G. Arulselvi<sup>3</sup>, D. Poornima<sup>4</sup>, J. Refonaa<sup>5</sup>, S. Dhamodaran<sup>5</sup>

<sup>1</sup> Associate Professor, Sathyabama Institute of Science and Technology, Chennai, India

<sup>2</sup> Professor, Sri Venkateswara College of Engineering, Sriperumbudur

<sup>3</sup> Associate Professor, Annamalai University, Chidambaram

<sup>4</sup> Research Scholar, Annamalai University, Chidambaram

<sup>5</sup> Assistant Professor, Sathyabama Institute of Science and Technology, Chennai, India

**Abstract:** The fusion of multimodal images is a trending research area, especially in the field of medical image processing. The purpose of image fusion is to classify medical images efficiently. The objective of the research work is to do the fusion of multimodal medical images for doing medical image classification. In this research, a new algorithm is proposed for the detection of brain tumors based on three main steps namely, fusion, segmentation, and classification. A sparse theory-based vector selection (STVS) algorithm is proposed for image fusion. In this algorithm, the multimodal images are first converted into patches. These patches are further vectorized. The vectorized patches are employed in the creation of dictionaries. The generated dictionaries along with the vectorized patches are used for the creation of sparse matrices. From the sparse matrices, a selection vector is formed using which the fused image is generated. The segmentation of the fused image is done using Intuitionistic fuzzy set-based k-means (IFSKM) clustering and the Otsu thresholding technique. The clusters of the IFSKM are generated based on the Intuitionistic fuzzy set (IFS) scheme. Finally, classification is performed based on a DCNN architecture. The proposed system is validated using the brain images from the Harvard Medical School. Quantitative analysis reveals that the proposed scheme achieves the best performance in terms of fusion, segmentation, and classification. The proposed STVS scheme attained high values of entropy, standard deviation, PSNR in dB, mean square error (MSE), structural similarity index (SSIM), and homogeneity with the values of 7.33, 55.25, 42.85, 0.098, 64.31, and 53.52 respectively.

**Keywords:** multimodal, fusion, segmentation, intuitionistic fuzzy set, structural similarity index, classification.

## 使用多模态医学图像融合检测脑肿瘤的备用理论

**摘要：**多模态图像的融合是一个趋势研究领域，尤其是在医学图像处理领域。图像融合的目的是对医学图像进行有效分类。研究工作的目标是进行多模态医学图像的融合以进行医学图像分类。在这项研究中，提出了一种基于融合、分割和分类三个主要步骤的脑肿瘤检测新算法。提出了一种基于稀疏理论的图像融合向量选择算法。在该算法中，首先将多模态图像转换为补丁。这些补丁被进一步矢量化。矢量化补丁用于创建字典。生成的字典以及矢量化补丁用于创建稀疏矩阵。从稀疏矩阵中，形成一个选择向量，使用该向量生成融合图像。融合图像的分割是使用基于直觉模糊集的 k-均值聚类和大津阈值技术完成的。基于直觉模糊

Received: 20 December, 2021 / Revised: 10 January, 2022 / Accepted: 21 February, 2022 / Published: 28 March, 2022

About the authors: S. L. Jany Shabu, Associate Professor, Sathyabama Institute of Science and Technology, Chennai, India; C. Jayakumar, Professor, Sri Venkateswara College of Engineering, Sriperumbudur; G. Arulselvi, Associate Professor, Annamalai University, Chidambaram; D. Poornima, Research Scholar, Annamalai University, Chidambaram; J. Refonaa, Assistant Professor, Sathyabama Institute of Science and Technology, Chennai, India; S. Dhamodaran, Assistant Professor, Sathyabama Institute of Science and Technology, Chennai, India;

Corresponding author S. L. Jany Shabu, [janyshabu.cse@sathyabama.ac.in](mailto:janyshabu.cse@sathyabama.ac.in)

集的 k-均值的集群是基于直觉模糊集 方案生成的。最后，基于深度卷积神经网络架构进行分类。所提出的系统使用来自哈佛医学院的大脑图像进行了验证。定量分析表明，该方案在融合、分割和分类方面取得了最佳性能。所提出的基于稀疏理论的向量选择方案的熵、标准差、峰值信噪比 ( dB )、均方误差、结构相似性指数和同质性值分别为 7.33、55.25、42.85、0.098、64.31 和 53.52。

**关键词：**多模态、融合、分割、直觉模糊集、结构相似性指数、分类。

## 1. Introduction

The mortality rate of brain tumors is constantly increasing since more people are getting affected by this disease. Thus, early detection of brain tumors is very essential to increase the survival rate of humans. Computer vision techniques are popularly being used in recent days for the assessment of brain images [1]. These techniques make use of image processing for the classification of brain images into various categories [2]. Automatic identification of malignant cases is a challenging task as the structural variation of the tumor regions is more identical to that of non-tumor regions. Various machine learning techniques are being used for the classification of brain images. These techniques perform classification in two steps namely, training and testing [3].

During the training stage, the labeled images are given to the classification algorithm to train and generate a classification model. This model is used during testing based on the testing data. Thus, the malignant images are identified from the benign images [4]. This classification is necessary as the malignant cases must be identified and treated at the earlier stages for the easy recovery of the patients with a brain tumor [5]. To increase the quality of classification steps like pre-processing, fusion and segmentation are performed with the brain image data. Precise identification of the brain tumor region is an important task as these regions contain the important information necessary for classification. This region identification is done using segmentation techniques [6].

The segmentation techniques usually employ clustering followed by thresholding. Clustering techniques employ routing of pixels that constitute similar features. Thresholding techniques are employed for the separation of tumor pixels from non-tumour pixels [7]. Two types of features are used for the representation of brain images. These include deep learning features and handcrafted features. The deep learning features are extracted using convolutional architectures [8].

In some cases, the combination of both types of cases is used for the classification. Due to the changes

in lifestyle, aging factors, and heredity reasons more and more populations are being affected by a brain tumors. Deep learning techniques employed pre-trained neural networks for the automatic generation of features [9]. Though benign tumor comprises non-cancer cells, their identification is also important since such abnormal tissues cause abnormal functioning of the brain. The treatment given for the cancerous and non-cancerous brain tumor cases are different, thus their identification is very important [10].

Various optimization techniques are also employed in tumor detection. These techniques employ algorithms based on bio-inspired techniques for the identification of malignant cases. These bio-inspired techniques use biological operations performed by various organisms as a base for the classification. Several quantities are optimized and the corresponding parameters are detected [11]. The computation of the computational complexity is vital since these algorithms must be implemented in real-time. Since many IoT-based devices are employed for the acquisition and transmission of data, real-time processing is done. Thus, computational time and computational complexity are important parameters considered in brain tumor detection [12].

In this research, we propose a new scheme for the detection of brain tumors using image fusion that is based on the sparse representation theory.

The overall contributions of this paper are fourfold:

- a) A new technique called sparse theory-based vector selection (STVS) technique for image fusion is presented.
- b) The segmentation of the fused image is done using a novel Intuitionistic fuzzy set-based k-means (IFSKM) clustering.
- c) Classification of the segmented clusters is done using a new DCNN architecture.
- d) Performance evaluation is done in terms of various fusion, segmentation, and classification metrics.

## 2. Literature Survey

Tan et al. [13] proposed a scheme for medical image fusion based on neural networks. A new fusion strategy

was proposed using energy as an attribute. Here, the images were first converted to the transform domain based on the non-subsampled Shearlet transform. The transform coefficients were then fused based on the energy content. Huang et al. [14] presented a review on various schemes available for image fusion. The main focus was provided on the usage of deep learning techniques for the combination of multimodal medical images. The popularly available medical image datasets were listed and the analysis of the various fusion techniques was done using popular fusion metrics.

Rajalingam et al. [15] utilized deep guided filtering algorithm for medical image fusion. Here, pathological features of the individual images were united. The images were decomposed based on frequencies. These components were then fused using the filtration technique to form filtered high-quality fused images. Arif et al. [16] used fast curvelet transform for the fusion of medical images. This transform was implemented using a genetic algorithm. The redundancy in the input images was fused based on the curvelet-based genetic methodology. After the application of the curvelet transform, the ridgelet transform was also applied to ensure the complete fusion of important features from the medical images.

Wang et al. [17] performed image fusion based on a contrast pyramid. The contrast pyramid features were extracted and fused based on CNN. The Siamese neural network was employed for the extraction of neural network features. The output of the neural network structure was used for the generation of the weight map that was utilized for the image fusion. Yadav et al. [18] utilized hybrid techniques for image fusion. The main advantages of multimodal imaging techniques were presented along with the advantages of multimodal image fusion. Further, the techniques employed for the fusion of images without the introduction of any flaws were also discussed. The usage of various analysis techniques in the denoising of the fused images was also analyzed.

Du et al. [19] presented a scheme for image fusion based on tensor features. The tensor features were extracted from the individual multimodal images and fused using three-layer image fusion techniques. The differential features were extracted based on the structure tensor components. These components were combined using a novel special frequency metric. Wang et al. [20] utilized sparse representation theory for the adaptive fusion of the medical images. Here, the input images were first split into four different images having varying sizes. The features required for the image fusion were extracted based on the Laplacian Pyramid theory. The noise components present in the higher frequency components were reduced based on the sparse representation.

Maqsood et al. [21] utilized sparse representation for the image fusion based on two-scale decomposition.

Initially, to increase the discriminative nature of the individual images, the contrast enhancement technique was employed. The enhanced images were then decomposed into two different components based on the detail and base nature. Finally, fusion was done using sparse theory. Chen et al. [22] presented a scheme for the combination of multimodal medical images using a Rolling guidance filter. The Rolling guidance filter was employed to split the medical images into structural and detail coefficients. These coefficients were then merged based on the Laplacian pyramid theory. This method attained better visual and quantitative fusion quality compared to other conventional systems.

Based on the different types of fusion techniques being surveyed, we have implemented a new fusion scheme in this research based on sparse theory and vector selection techniques.

### 3. Proposed Methodology

The proposed methodology comprises three main stages namely, multimodal medical image fusion, image segmentation, and classification. This is depicted in Fig. 1. In this research, we have employed a new technique called the sparse theory-based vector selection (STVS) technique for image fusion. The segmentation of the fused image is done using Intuitionistic fuzzy set-based k-means clustering (IFSKM) clustering and Otsu thresholding technique. Finally, classification is done using DCNN architecture.

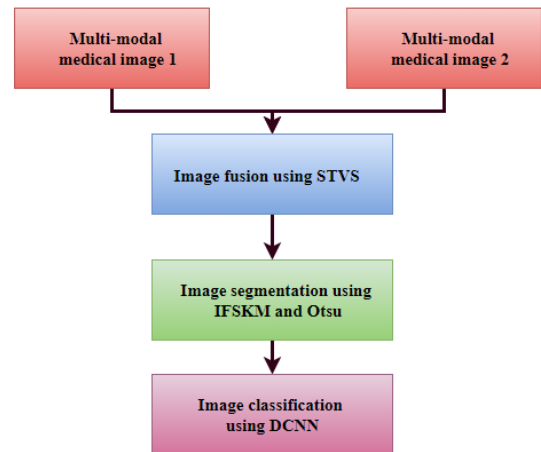


Fig. 1 Flow chart of the proposed methodology

#### 3.1. Image Fusion using Sparse Theory-Based Vector Selection (STVS) Technique

The proposed image fusion scheme makes use of sparse theory. The proposed algorithm is represented by Algorithm 1. In this scheme, two input images are considered namely, the multimodal image 1  $MI1 \in \mathbb{R}^{M \times N}$  and multimodal image 2  $MI2 \in \mathbb{R}^{M \times N}$ . Initially, the first image is converted to patches  $p_1^1, p_2^1, p_3^1, \dots, p_n^1$  of size  $n \times n$ . Then, similar to the first image, the second image is also converted to patches

$p_1^2, p_2^2, p_3^2, \dots, p_n^2$  of size  $n \times n$ . These patches are then vectorized to form vectors of size  $n \times 1$ . The generated vectors are then appended to form vector matrices namely  $VM^1 \in R^{n^2 \times P}$  and  $VM^2 \in R^{n^2 \times P}$ . Dictionary learning was done using the ODL algorithm for dictionaries DI1 and DI2 using VM1 and VM2. The vector-matrix VM1 and dictionary DI1 are then used to compute the sparse matrix SM1 using the LARS technique. Similarly, the vector-matrix VM2 and dictionary DI2 are used to compute the sparse matrix SM2. The selection vector  $SV = \{sv1, sv2, \dots, svp\}$  is then generated based on the l-1 norm value of the sparse matrices. Using the selection vector, the fused vector matrix  $VM^F = \{vf_1^F, vf_2^F, \dots, vf_p^F\}$  is formed. Finally, the fused image  $FI \in RM \times N$  is formed using the patches selected from the fused vector. The entire process is explained in four main steps below.

### 3.1.1 Patch Vectorization

Initially, the input multimodal image 1  $MI1 \in RM \times N$  and multimodal image 2  $MI2 \in RM \times N$  are converted to patches  $p_1^1, p_2^1, p_3^1, \dots, p_n^1$  and  $p_1^2, p_2^2, p_3^2, \dots, p_n^2$  respectively. Here,  $N$  refers to the total number of patches. The patch conversion is done using the sliding window technique. In this work, we have employed a sliding window of size  $n \times n$  without overlap. This is employed to reduce the overall computation complexity of the sparse coding and dictionary learning steps. The  $i$ th patch of the image  $MI1$  and image  $MI2$  are represented as  $p_i^1$  and  $p_i^2$  respectively. These patches are then converted to vectors of size  $n \times 1$ . This process is done using the patch vectorization technique, in which each squared patch is converted to a column vector of length  $n^2$ .

### 3.1.2. Edge Matrix Computation

In the case of multimodal medical images, it is evident that each image contains complimentary information. For instance, in the case of MRI and CT images, the MRI images represent the soft tissue regions and the CT images represent the bone regions. Thus, the identification of edge information aids in the identification of patches that contain more information. In our work, the edge matrices are computed based on the Histogram of Oriented Gradients (HOG) technique. This helps in the identification of the patch that has more salient information. The HOG descriptor converts the image patch into  $L$  different orientation bins. These bins are represented as  $p_1, p_2, \dots, p_L$ . These bins are oriented such that they are spaced equally within the angular region of  $00-1800$ . Then, for the patch  $p_i^k, k \in 1, 2$ , the  $j$ th orientation bin is represented using the following equation (1),

$$G_i(\rho_j), j \in 1, 2, \dots, L. \quad (1)$$

### 3.1.3: Dictionary learning and Sparse coding

The sparse representation modeling technique is popularly employed in the field of image fusion. This modeling technique has extraordinary signal representation capabilities. Using this modeling, the over-complete dictionaries can be generated. In this work, we have used the online dictionary learning (ODL) algorithm. This algorithm is based on a convex relaxation technique. Consider the edge matrix  $EM_k, k \in 1, 2$  that can be represented as  $EM_k = [em_1, em_2, \dots, em_k]$ . The optimization function for dictionary generation is given by,

$$\min_{DI^k, \sigma} \frac{1}{K} \sum_{i=1}^K \left( \frac{1}{2} \|em_i - DI^k \sigma_i\|_2^2 + \lambda \|\sigma_i\|_1 \right) \quad (2)$$

Where  $DI_k, k \in 1, 2$  represents the dictionaries for image 1 and image 2 respectively. Further,  $\sigma = [\sigma_1, \sigma_2, \dots, \sigma_k]$  represents the sparse coefficients and  $\lambda$  is the regularization parameter. Using the generated dictionaries, sparse matrices  $SM^1 = \{sm_1^1, sm_2^1, \dots, sm_p^1\}$   $p_i^k, k \in 1, 2$  and  $SM^2 = \{sm_1^2, sm_2^2, \dots, sm_p^2\}$  are formed using the Least angle regression (LARS) algorithm. In this algorithm, the sparse coding step is performed using

$$sm_i \square \arg \min_{sm} \frac{1}{2} \|em_i - DI_{t-1} sm\|_2^2 + \lambda \|sm\|_1 \quad (3)$$

Where  $t$  represents the iteration number and  $t < T$  where  $T$  is the total number of iterations. The generated sparse matrices are used for the creation of a selection vector. The selection vector selection vector  $SV = \{sv1, sv2, \dots, svP\}$  is generated by comparing the magnitude of the sparse matrices of the two multimodal images.

### 3.1.4. Fusion Rule

Using the selection vector, the fused vector matrix  $VM^F = \{vf_1^F, vf_2^F, \dots, vf_p^F\}$  is formed. Each value of the fused vector-matrix either has a value of 1 or a value of 2. Value 1 indicates the patch from the multi-modal image 1 and a value of 2 represents the patch from the multi-modal image 2. The fused vectors are then converted to patches to form the fused image  $FI \in RM \times N$ . This conversion is done similar to the initial patch vectorization step but in a reverse manner. The overall framework of image fusion using the STVS technique is illustrated in Fig. 2.

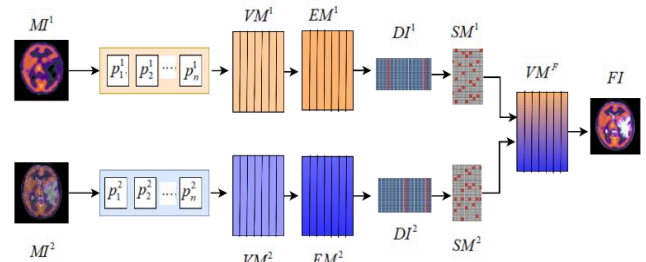


Fig. 2. The overall framework of image fusion using the STVS technique



Algorithm 1: Proposed sparse theory-based vector selection (STVS) technique.

*Input:* Multimodal image 1  $MI1 \in RM \times N$  and multimodal image 2  $MI2 \in RM \times N$ .

*Output:* Fused image  $FI \in RM \times N$ .

*Steps:*

- The input multimodal image 1 is converted to patches  $p_1^1, p_2^1, p_3^1, \dots, p_n^1$  of size  $n \times n$ .

- The input multimodal image 2 is converted to patches  $p_1^2, p_2^2, p_3^2, \dots, p_n^2$  of size  $n \times n$ .

- The patches of image 1 and image 2 are vectorized to form vectors of size  $n2 \times 1$ .

- The formed vectors are then appended to form vector matrices namely  $VM^1 \in R^{n^2 \times P}$  and  $VM^2 \in R^{n^2 \times P}$ .

- Compute edge matrices for EM1 and EM2 using VM1 and VM2 respectively using Histogram of Oriented Gradients [23].

- Using ODL [24] algorithm form dictionaries DI1 and DI2 using EM1 and EM2 respectively.

- Using vector-matrix VM1 and dictionary DI1 compute the sparse matrix using LARS [25] technique.

$$SM^1 = \{sm_1^1, sm_2^1, \dots, sm_p^1\} \quad (4)$$

- Similarly, using vector-matrix VM2 and dictionary DI2 compute the sparse matrix.

$$SM^2 = \{sm_1^2, sm_2^2, \dots, sm_p^2\} \quad (5)$$

- Form the selection vector  $SV = \{sv1, sv2, \dots, svP\}$  using

$$sv_i = \begin{cases} 1; & \text{if } |sm_i^1| > |sm_i^2| \\ 2; & \text{if } |sm_i^2| > |sm_i^1| \end{cases} \quad (6)$$

Where  $i = 1, 2, \dots, P$ .

- Form the fused vector-matrix  $VM^F = \{vf_1^F, vf_2^F, \dots, vf_p^F\}$

$$vf_i^F = \begin{cases} sm_i^1; & \text{if } sv_i = 1 \\ sm_i^2; & \text{if } sv_i = 2 \end{cases} \quad (7)$$

Where  $i = 1, 2, \dots, P$ .

- Convert the fused vectors to patches to form the fused image

$FI \in RM \times N$ .

### 3.2. Tumor Segmentation using Intuitionistic Fuzzy Set-Based K-means Clustering (IFSKM)

Clustering based on the k-means technique is popularly employed in image segmentation. In this technique, the image is divided into k number of clusters. The regions having similar features are grouped as a single cluster. In the k-means algorithm, the initial k cluster centroids are referred to as the following:

$$CE = \{Ce_i / i = 1, 2, \dots, k\} \quad (8)$$

The main drawback of the k-means clustering is the random selection of the initial centroid. In the proposed segmentation scheme, the initial selection is done based on the Intuitionistic fuzzy set (IFS) scheme. In the IFS scheme, data Y is represented as

$$IFS = \{y, \eta(y), \lambda(y); y \in Y\} \quad (9)$$

$\eta(y)$  represents the degree of belongingness of y in Y and  $\lambda(y)$  is the degree of non-belongingness of y in Y.

In the above equation, we find that

$$0 \leq \eta(y) + \lambda(y) \leq 1 \quad (10)$$

In the proposed IFSKM scheme, the initial centroids are selected such that

$$CE = \{ce_i, \eta(ce_i), \lambda(ce_i); ce_i \in CE\} \quad (11)$$

The clustered regions were then segmented based on the Otsu thresholding scheme to form the segmented regions.

### 3.3. Classification

The segmented image slices were then given as input to the DCNN structure. This architecture is shown in Figure 3. This structure comprises of pre-trained GoogleNet, fully connected layers, and the Long Short Term Memory (LSTM) classification structure. The images were classified into two categories namely, benign and malignant. The GoogleNet is comprised of several filters of varying sizes. The first layer is comprised of filters of size  $224 \times 224$ . The second layer represented filters of size  $112 \times 112$ . The third layer consisted of filters of size  $56 \times 56$  and the fourth layer utilized filters of size  $28 \times 28$ . In the final two layers, filters of sizes  $14 \times 14$  and  $7 \times 7$  were employed. The output of these layers was given as input to the fully connected block (FC) that comprised of 2 layers. These layers are comprised of 4096 nodes each. Finally, classification was done using an LSTM structure to detect the malignant cases. The main use of using the GoogleNet structure for pre-training is because it produces a minimal error of about 5.5%.

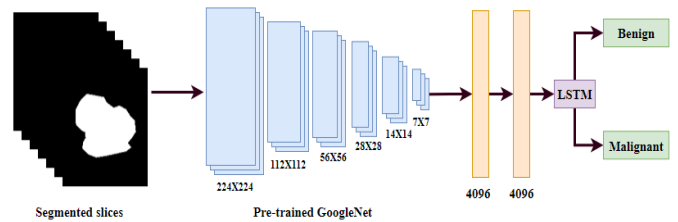


Fig. 3 The architecture of the proposed Deep Convolutional Neural Network

## 4. Results and Discussion

The proposed framework was evaluated using both qualitative and quantitative analysis. The qualitative analysis was done to assess the performance of the proposed fusion algorithm visually. The appearance of the fused image was compared visually with that of the individual multimodal images. This was done to

evaluate the structural integrity of the fused images. In the quantitative analysis, the proposed framework was evaluated based on fusion, segmentation, and classification algorithms. The proposed STVS fusion algorithm was compared with popular fusion algorithms like 2D discrete wavelet transform (DWT), 2D stationary wavelet transforms (SWT) and non-subsampled contourlet transforms (NSCT). This evaluation was done using fusion metrics like spatial frequency, standard deviation, Mutual information, Qydeas's (QAB/F) fusion metric, Mean structural similarity (MSSIM), and Piella's fusion metric. The proposed IFSKM segmentation algorithm was evaluated quantitatively in terms of metrics like Jaccard and Dice coefficient. Algorithms like the k-means algorithm and watershed algorithm were used for comparison with the proposed segmentation algorithm. The classification performance of the DCNN algorithm was assessed by comparison with algorithms like k-nearest neighbor (k-NN), Random Forest (RF), support vector machine (SVM), and sparse representation-based classification (SRC).

## 5. Strengths and Limitations

- The sparse domain-based technique has the benefits of good strength and low distortion, but it also produces noise during fusion computation. As a result, image fusion faces a de-noising issue.

- Sparse Representation approaches have acquired a lot of traction in the transform area, and they've shown to be effective in medical image analysis. However, these approaches have flaws, such as 1st one when different modalities are collected from the source images, the fusion rule causes spatial inconsistencies in the fused image.

- Due to the training and optimization of the dictionaries, the filters employed for SR-based picture fusion are time-dependent, and these algorithms are also unable to dissect several types of images.

- Another constraint is the complex orientated shape of source images, which cannot be correctly classified using an existing lexicon.

- While research in the field of multi-modal image fusion has yielded promising results, there are some limitations.

- Additionally, a morphological ensemble classification model based on SR for pixel-level picture fusion. However, the proposed model's efficiency is reduced by the blurring effect during deconstruction.

### 5.1. Parameter Settings

Six pairs of brain multimodal images were considered for analysis of our work. The value of patch size  $n$  was chosen to be 8. The brain images employed in this research were obtained from Harvard Medical School

(<https://www.med.harvard.edu/aANliB/home.html>).

The value of the regularization parameter  $\lambda$  was set as 0.5. The total number of iterations  $T$  in the LARS algorithm was chosen as 100.

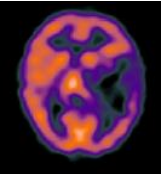
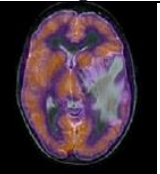
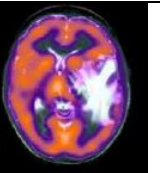
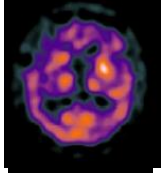
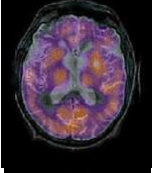
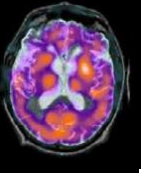



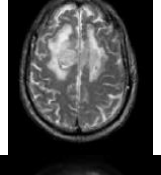
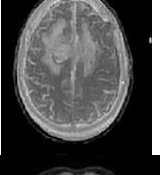
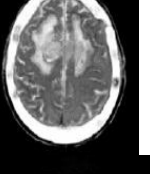
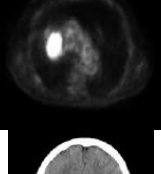
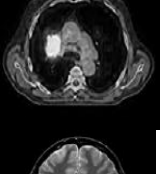
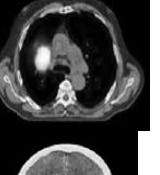


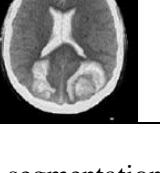
### 5.2. Experimental Setup

All the experiments done in this work were accomplished with Matlab R2014b using a Laptop with Intel core i5 @4 GHz using 6GB RAM.

### 5.3. Qualitative Analysis

Table 1 depicts the six different input source multimodal images and the corresponding fusion results obtained using the proposed STVS fusion algorithm. From Table 1, it can be visually observed that the fusion result has very good quality. It represents the important features from both the input images. This helps to improve the accuracy of segmentation, thereby, increasing the quality of classification.

Table 1. The source multimodal images and the fusion results

No	Multimodal image 1	Multimodal image 2	Fused image
1			
2			
3			
4			
5			
6			

The fused images are subjected to segmentation using the proposed IFSKM clustering and Otsu

thresholding algorithms. These are shown in Fig. 4. The segmentation results clearly show the region containing the tumor regions. The segmented regions are given as slice inputs to the DCNN architecture that is used for the classification of brain images into two categories namely, benign and the malignant category.

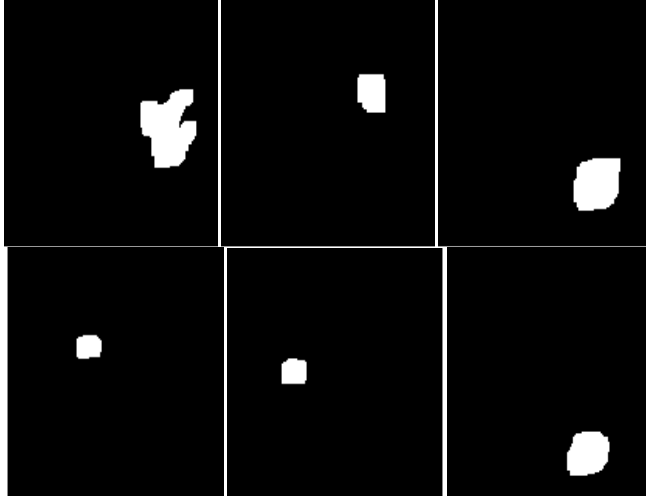


Fig. 4 Segmentation results were obtained for the 6 fused images using IKSKM clustering and Otsu thresholding

The results of image fusion studies are shown in Figure 4. By analyzing the partially expanded image, the fused image created by the suggested method has a good general visualization capability and a high image contrast. The suggested enhancement algorithm produces high-brightness fused pictures. Both approaches perform poorly in the preservation of image details, as evidenced by the partial enlargements marked in green and red dashed frames. The specific information of the image edge is not apparent, according to the details assessment, which is not good for human eye observing. When compared to the source image, the fused image produced by the suggested technique has a poor resemblance to the source image and does not well retain the source image's precise local structure. In some locations, the suggested method's fused image is too smooth, and the detailed image texture is not visible enough. The suggested method produces a brilliant fused image that does not properly maintain the detailed elements of the original images. The presented scheme produced the fused image shown in Figure 4, which has a high edge brightness, which degrades the detailed texture features of object boundaries.

#### 5.4. Quantitative Analysis

In this research, analysis was performed for evaluating the performance of the proposed fusion, segmentation, and classification algorithms.

##### 5.4.1. Evaluation of Proposed Fusion Methodology

The proposed fusion methodology is evaluated using metrics like spatial frequency, standard deviation, Mutual information, Qydeas's (QAB/F) fusion metric,

Mean structural similarity (MSSIM), and Piella's fusion metric.

Table 2 shows the variation of spatial frequency for the 2D DWT, 2D SWT, NSCT, and the proposed STVS algorithm. It is observed that the overall average value of spatial frequency achieved for all the 6 images using discrete wavelet transform is 18.08. The average value of spatial frequency for the stationary wavelet transform is 19.08 and that for the non-subsampled contourlet transform is 20.67. The proposed STVS fusion scheme attains the highest spatial frequency of 22.40.

Table 2 Spatial frequency for evaluation of image fusion

Image Set	Spatial frequency			
	2D Discrete Wavelet Transform	2D Stationary Wavelet Transform	Non-Subsampled Contourlet Transform	Proposed STVS
1	17.43	17.99	20.99	22.41
2	18.64	18.47	21.43	22.64
3	19.65	18.93	20.48	21.64
4	17.89	19.74	19.86	21.95
5	16.94	19.70	19.93	23.21
6	17.94	19.67	21.34	22.58

Table 3 shows the variation of standard deviation for the 2D DWT, 2D SWT, NSCT, and the proposed STVS algorithm. It is observed that the overall average value of standard deviation achieved for all the 6 images using discrete wavelet transform is 35.40. The average value of standard deviation for the stationary wavelet transform is 36.46 and that for the non-subsampled contourlet transform is 38.38. The proposed STVS fusion scheme attains the highest standard deviation of 43.17.

Table 3 Standard deviation for evaluation of image fusion

Image Set	Standard deviation			
	2D Discrete Wavelet Transform	2D Stationary Wavelet Transform	Non-Subsampled Contourlet Transform	Proposed STVS
1	35.23	36.94	37.83	40.52
2	36.53	36.84	37.65	41.53
3	34.13	35.32	38.95	45.37
4	36.32	35.95	38.32	46.23
5	34.98	36.83	38.63	44.55
6	35.24	36.93	38.93	40.85

Table 4 shows the variation of mutual information (MI) for the 2D DWT, 2D SWT, NSCT, and the proposed STVS algorithm. It is observed that the overall average value of MI achieved for all the 6 images using discrete wavelet transform is 3.41. The average value of MI for the stationary wavelet transform is 3.56 and that for the non-subsampled contourlet transform is 3.66. The proposed STVS fusion scheme attains the highest mutual information of 4.24.

Table 4 Mutual information for evaluation of image fusion

Image Set	Mutual information			Proposed STVS
	2D Discrete Wavelet Transform	2D Stationary Wavelet Transform	Non-Subsampled Contourlet Transform	
1	3.21	3.46	3.64	4.21
2	3.12	3.65	3.86	4.15
3	3.53	3.56	3.74	4.36
4	3.47	3.85	3.86	4.26
5	3.66	3.24	3.63	4.27
6	3.47	3.64	3.25	4.19

Table 5 shows the variation of Qydeas's (QAB/F) fusion metric for the 2D DWT, 2D SWT, NSCT, and the proposed STVS algorithm. It is observed that the overall average value of Qydeas's (QAB/F) fusion metric achieved for all the 6 images using discrete wavelet transform is 0.563. The average value of Qydeas's (QAB/F) fusion metric for the stationary wavelet transform is 0.607 and that for the non-subsampled contourlet transform is 0.665. The proposed STVS fusion scheme attains the highest Qydeas's (QAB/F) fusion metric of 0.755.

Table 5 Qydeas's (QAB/F) fusion metric for evaluation of image fusion

Image Set	QAB/F			Proposed STVS
	2D Discrete Wavelet Transform	2D Stationary Wavelet Transform	Non-Subsampled Contourlet Transform	
1	0.525	0.634	0.629	0.723
2	0.554	0.568	0.694	0.784
3	0.582	0.593	0.663	0.734
4	0.539	0.612	0.635	0.764
5	0.584	0.615	0.689	0.783
6	0.599	0.624	0.681	0.742

Table 6 shows the variation of mean structural similarity (MSSIM) for the 2D DWT, 2D SWT, NSCT, and the proposed STVS algorithm. It is observed that the overall average value of mean structural similarity achieved for all the 6 images using discrete wavelet transform is 0.678. The average value of mean structural similarity for the stationary wavelet transform is 0.742 and that for the non-subsampled contourlet transform is 0.768. The proposed STVS fusion scheme attains the highest mean structural similarity of 0.867.

Table 6 Mean structural similarity (MSSIM) for evaluation of image fusion

Image Set	MSSIM			Proposed STVS
	2D Discrete Wavelet Transform	2D Stationary Wavelet Transform	Non-Subsampled Contourlet Transform	
1	0.679	0.753	0.789	0.841
2	0.684	0.785	0.743	0.866
3	0.694	0.732	0.794	0.854
4	0.695	0.714	0.785	0.863
5	0.663	0.743	0.763	0.886
6	0.653	0.726	0.734	0.896

Table 7 shows the variation of Piella's fusion metric for the 2D DWT, 2D SWT, NSCT, and the proposed STVS algorithm. It is observed that the overall average value of Piella's fusion metric achieved for all the 6 images using discrete wavelet transform is 0.578. The average value of Piella's fusion metric for the stationary wavelet transform is 0.630 and that for the non-subsampled contourlet transform is 0.655. The proposed STVS fusion scheme attains the highest Piella's fusion metric of 0.767.

Table 7 Piella's fusion metric for evaluation of image fusion

Image Set	Piella's fusion metric			
	2D Discrete Wavelet Transform	2D Stationary Wavelet Transform	Non-Subsampled Contourlet Transform	Proposed STVS
1	0.582	0.614	0.673	0.784
2	0.573	0.625	0.649	0.756
3	0.583	0.635	0.639	0.776
4	0.586	0.618	0.694	0.759
5	0.556	0.628	0.649	0.788
6	0.585	0.662	0.629	0.740

#### 5.4.2. Segmentation Technique Evaluation

We have evaluated the proposed segmentation scheme in terms of the Jaccard and Dice coefficient. Table 8 shows the comparison of the Jaccard coefficient for the considered 6 images. It can be seen that the average Jaccard coefficient for the k-means algorithm is 0.5591. The average Jaccard coefficient for the watershed algorithm is 0.626. However, the average Jaccard coefficient for the proposed IFSKM algorithm is 0.7555. Thus, IFSKM achieves the best performance in terms of the Jaccard coefficient.

Table 8. Performance evaluation using Jaccard Coefficient

Image Set	Jaccard Coefficient		
	K-means algorithm	Watershed algorithm	Proposed IFSKM
1	0.553	0.623	0.743
2	0.562	0.540	0.775
3	0.522	0.616	0.735
4	0.567	0.637	0.727
5	0.562	0.688	0.789
6	0.589	0.652	0.764

Table 9 shows the comparison of the Dice coefficient for the considered 6 images. It can be seen that the average Dice coefficient for the k-means algorithm is 0.6111. The average Dice coefficient for the watershed algorithm is 0.6693. However, the average Dice coefficient for the proposed IFSKM algorithm is 0.7796. Thus, we infer that IFSKM produces the best results in terms of the Dice coefficient.



Table 9 Performance evaluation using Dice Coefficient

Image Set	Dice Coefficient		
	K means algorithm	Watershed algorithm	Proposed IFSKM
1	0.562	0.698	0.754
2	0.624	0.637	0.743
3	0.666	0.653	0.876
4	0.613	0.697	0.746
5	0.623	0.674	0.784
6	0.579	0.657	0.775

Table 10 shows the comparison of structural similarity index (SSIM) for the considered 6 images. It can be seen that the average SSIM for the k-means algorithm is 0.756. The average SSIM for the watershed algorithm is 0.868. However, the average SSIM for the proposed IFSKM algorithm is 0.941. Thereby, we can say that the SSIM of the proposed IFSKM is the best.

Table 10 Performance evaluation using SSIM

Image Set	SSIM		
	K means algorithm	Watershed algorithm	Proposed IFSKM
1	0.734	0.898	0.942
2	0.752	0.887	0.912
3	0.766	0.812	0.953
4	0.723	0.894	0.947
5	0.773	0.865	0.977
6	0.789	0.852	0.917

#### 5.4.3. Evaluation of Classification Algorithms

The classification performance of the DCNN algorithm was evaluated by comparison with algorithms like k-NN, RF, SVM, and SRC. Table 11 shows the comparison of overall accuracy. From Table 11, it is clear that the accuracy of k-NN is 79.32%. The accuracy achieved by RF is 83.12% and that of SVM is 91.58%. The accuracy of SRC is 91.58%. However, the proposed DCNN has the highest accuracy of 94.93%.

Table 11. Comparison of Overall Accuracy

Classification algorithm	Overall classification accuracy (%)
k-NN	79.32
RF	83.21
SVM	89.37
SRC	91.58
DCNN	94.93

Fig. 5 shows the comparison of overall specificity. From Figure 4, it is clear that the specificity of k-NN is 81.23%. The specificity achieved by RF is 83.72% and that of SVM is 85.46%. The specificity of SRC is 88.74%. However, the proposed DCNN has the highest specificity of 94.82%.

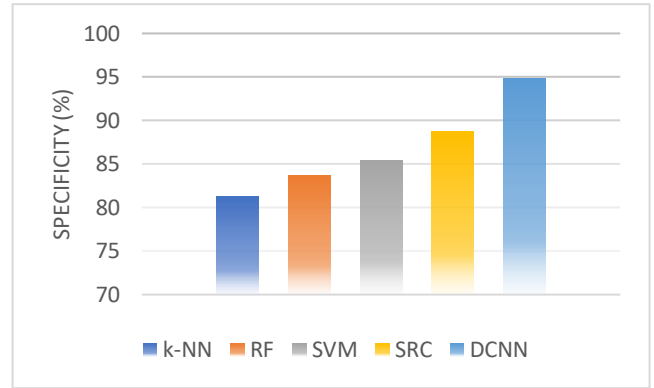


Fig. 5 Comparison of specificity

Fig. 6 shows the comparison of overall precision. From Figure 5, it is clear that the precision of k-NN is 78.32%. The precision achieved by RF is 81.43% and that of SVM is 85.83%. The precision of SRC is 89.65%. However, the proposed DCNN has the highest precision of 95.37%.

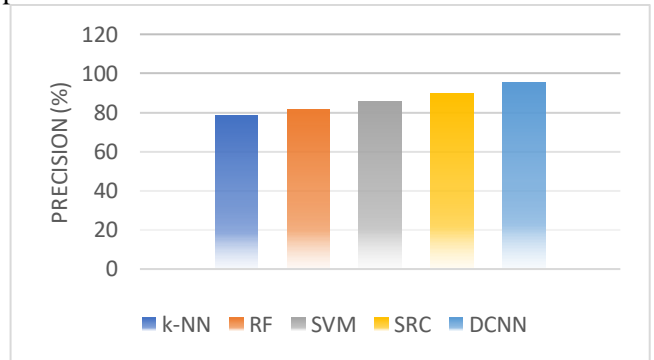


Fig. 6 Comparison of precision

Fig. 7 shows the comparison of overall recall. From Figure 6, it is clear that the recall of k-NN is 83.78%. The recall achieved by RF is 85.93% and that of SVM is 89.73%. The recall of SRC is 91.37%. However, the proposed DCNN has the highest recall 93.82%.

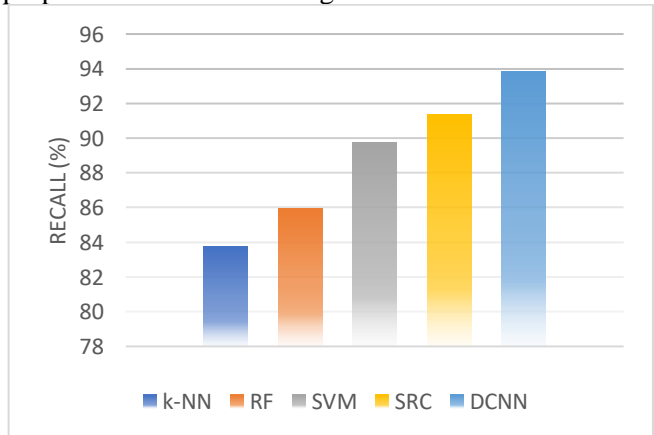


Fig. 7 Comparison of recall

Fig. 8 shows the comparison of the F-score. From Figure 7, it is clear that the F-score of k-NN is 79.42%. The F-score achieved by RF is 84.82% and that of SVM is 88.57%. The F-score of SRC is 90.94%. However, the proposed DCNN has the highest F-score of 93.72%.

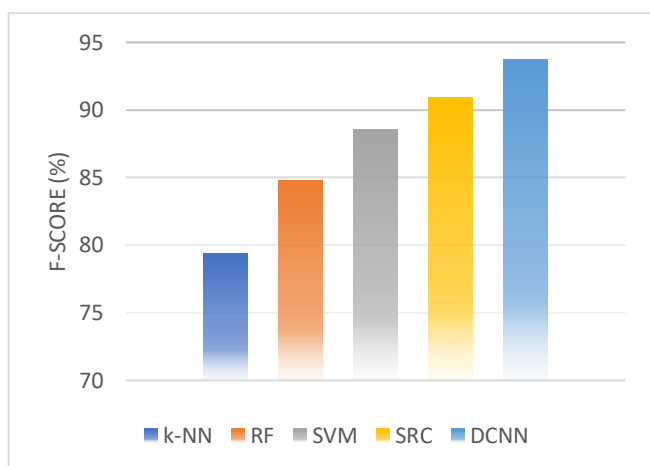


Fig. 8 Comparison of F-score

Table 12 shows the comparison of overall classification time. From Table 12, it is clear that the classification time of k-NN is 29.57ms. The classification time achieved by RF is 21.43ms and that of SVM is 18.32ms. The classification time of SRC is 10.74ms. However, the proposed DCNN has a minimal classification time of 8.56ms. Since this time is very less, the proposed scheme can be easily implemented in real-time applications.

Table 12 Comparison of classification time

Classification algorithm	Classification time (ms)
k-NN	29.57
RF	21.43
SVM	18.32
SRC	10.74
DCNN	8.56

## 6. Advantage of the Proposed Methodology

The main advantage of the proposed methodology is the improved fusion performance. This helps to form fused images that have complementary information from both the input images. The other advantage is the high quality of segmentation obtained using the proposed segmentation algorithm. Further, we have attained the highest accuracy in the detection and classification of brain tumors.

## 7. Drawback of the Proposed Methodology

The only drawback of the proposed scheme is the increased complexity of the image fusion algorithm.

## 8. Conclusion

Medical images of many forms can aid in the accurate detection of diseases. X-rays, CT scans, MRIs, and PET scans are examples of common medical imaging procedures [26-29]. Due to the obvious various imaging methods, there are considerable disparities in the attention being paid to various modal

medical images of individual organs and tissues. When it comes to the diagnosis of diseases, single-type images frequently fall short of offering advanced and appropriate information. To diagnose a patient's condition, clinicians must typically synthesize numerous distinct kinds of medical images from the same perspective, which is inconvenient and decreases diagnostic performance. Multi-modal medical picture fusion has been efficiently applied to medical diagnosis as a response to these challenges. Multi-modal medical image fusion integrates data from several kinds of medical images and shows the integrated image in a fused image as a key benefit. Because of its broad built-in library compatibility, state-of-the-art approaches for multimodal imagery fusion use MATLAB R2020b (MathWorks Inc., MA, USA) to generate simulated results. Microsoft Windows 10 is installed on a computing system that contains an Intel Core i7 9750H 2.59 GHz processor and 16 GB of memory. The multimodal brain image datasets consisting of CT and MR images were acquired. Each of the given datasets has 500 grayscale images chosen for measuring performance. The dimensions of the input photos are standardized at 256 x 256 pixels.

The images created by our proposed method were compared to the images generated by the preceding algorithms utilizing different datasets, namely Data-1 through Data-6. The proposed method is evaluated to the Discrete Wavelet Transform (DWT), dual-tree complex wavelet transforms (DTCWT), non-subsampled contourlet transform (NSCT), Convolutional Neural Network (CNN), and the proposed algorithm for graphical quality assessment of the Data-1 dataset. An MRI image shows information about soft tissues, whereas a CT image shows data about hard tissues and their architecture. It is crucial to combine important information from the preceding photos into a single fused image for better identification. The stated collection of algorithms performs multimodal image fusion in this approach. The qualitative results show that DWT, DTCWT, NSCT, and CNN perform poorly in terms of contrast and visual effect. It's worth noting that these algorithms can't preserve data in the fused image, which corresponds to the appropriate assessment metric MI, which is related to the concentration of extracting information.

In this research, we have proposed a new technique for the detection of brain tumors based on image fusion, segmentation, and classification. Image fusion was performed using a new technique called the sparse theory-based vector selection (STVS) technique. The segmentation of the tumor regions from the fused images was performed using Intuitionistic fuzzy set-based k-means clustering (IFSKM) clustering and the Otsu thresholding technique. Finally, the segmented results were classified using a new DCNN architecture.

The proposed DCNN architecture is comprised of a pre-trained GoogleNet structure, fully connected layers, and the LSTM classification structure. The images were classified into two categories namely, benign and malignant. The average Jaccard coefficient for the proposed IFSKM algorithm was 0.7555. Similarly, the average Dice coefficient for the proposed IFSKM algorithm was 0.7796. It was also shown that the classification performance of the proposed DCNN classification framework was high with a value of 94.93% accuracy, 94.82% specificity, 95.37% precision, 91.37% recall, and 93.72% F-score.

### 8.1. Future Work

In the future, we have planned to implement image fusion based on the combination of Laplacian pyramid and sparse representation theory to enhance the quality of image fusion so that the accuracy of brain tumor detection is enhanced.

## References

- [1] JALALI V., & KAUR D. A study of classification and feature extraction techniques for brain tumor detection. *International Journal of Multimedia Information Retrieval*, 2020, 9(4): 271–290. <https://doi.org/10.1007/s13735-020-00199-7>
- [2] SABA T., SAMEH MOHAMED A., EL-AFFENDI M., AMIN J., and SHARIF M. Brain tumor detection using fusion of hand crafted and deep learning features. *Cognitive Systems Research*, 2020, 59: 221–230. <https://doi.org/10.1016/j.cogsys.2019.09.007>
- [3] SHARIF M., AMIN J., RAZA M., ANJUM M. A., AFZAL H., and SHAD S. A. Brain tumor detection based on extreme learning. *Neural Computing and Applications*, 2020, 32(20): 15975–15987. <https://doi.org/10.1007/s00521-019-04679-8>
- [4] BAI X., ZHOU F., and XUE B. Fusion of infrared and visual images through region extraction by using multi scale center-surround top-hat transform. *Optics Express*, 2011, 19(9): 8444. <https://doi.org/10.1364/oe.19.008444>
- [5] AMIN J., SHARIF M., RAZA M., SABA T., SIAL R., and SHAD S. A. Brain tumor detection: a long short-term memory (LSTM)-based learning model. *Neural Computing and Applications*, 2020, 32(20): 15965–15973. <https://doi.org/10.1007/s00521-019-04650-7>
- [6] CHAHAL P. K., PANDEY S., and GOEL S. A survey on brain tumor detection techniques for MR images. *Multimedia Tools and Applications*, 2020, 79(29–30): 21771–21814. <https://doi.org/10.1007/s11042-020-08898-3>
- [7] SHARIF M., AMIN J., NISAR M. W., ANJUM M. A., MUHAMMAD N., and ALI SHAD S. A unified patch based method for brain tumor detection using features fusion. *Cognitive Systems Research*, 2020, 59: 273–286. <https://doi.org/10.1016/j.cogsys.2019.10.001>
- [8] RAJINIKANTH V., RAJ A.N.J., THANARAJ K. P., and NAIK G. R. A customized VGG19 network with concatenation of deep and handcrafted features for brain tumor detection. *Applied Sciences*, 2020, 10(10). <https://doi.org/10.3390/app10103429>
- [9] WINDISCH P., WEBER P., FÜRWEGER C., EHRET F., KUFELD M., ZWAHLEN D., and MUACEVIC A. Implementation of model explainability for a basic brain tumor detection using convolutional neural networks on MRI slices. *Neuroradiology*, 2020, 62(11): 1515–1518. <https://doi.org/10.1007/s00234-020-02465-1>
- [10] CHANDRAS.K., and BAJPAI M. K. Fractional Crank-Nicolson finite difference method for benign brain tumor detection and segmentation. *Biomedical Signal Processing and Control*, 2020, 60: 102002. <https://doi.org/10.1016/j.bspc.2020.102002>
- [11] SHARIF M., AMIN J., RAZA M., YASMIN M., and SATAPATHY S. C. An integrated design of particle swarm optimization (PSO) with fusion of features for detection of brain tumor. *Pattern Recognition Letters*, 2020, 129: 150–157. <https://doi.org/10.1016/j.patrec.2019.11.017>
- [12] KHAN S. R., SIKANDAR M., ALMOGREN A., UD DIN I., GUERRIERI A., and FORTINO G. IoMT-based computational approach for detecting brain tumor. *Future Generation Computer Systems*, 2020, 109: 360–367. <https://doi.org/10.1016/j.future.2020.03.054>
- [13] TAN W., TIWARI P., PANDEY H. M., MOREIRA C., and JAISWAL A. K. Multimodal medical image fusion algorithm in the era of big data. *Neural Computing and Applications*, 2020. <https://doi.org/10.1007/s00521-020-05173-2>
- [14] HUANG B., YANG F., YIN M., MO X., and ZHONG C. A Review of Multimodal Medical Image Fusion Techniques. *Computational and Mathematical Methods in Medicine*, 2020: 8279342. <https://doi.org/10.1155/2020/8279342>
- [15] RAJALINGAM B., AL-TURJMAN F., SANTHOSHKUMAR R., and RAJESH M. Intelligent multimodal medical image fusion with deep guided filtering. *Multimedia Systems*, 2020: 0123456789. <https://doi.org/10.1007/s00530-020-00706-0>
- [16] ARIFM., and WANG G. Fast curvelet transform through genetic algorithm for multimodal medical image fusion. *Soft Computing*, 2020, 24(3): 1815–1836. <https://doi.org/10.1007/s00500-019-04011-5>
- [17] WANG K., ZHENG M., WEI H., QI G., and LI Y. Multi-modality medical image fusion using convolutional neural network and contrast pyramid. *Sensors*, 2020, 20(8): 1–17. <https://doi.org/10.3390/s20082169>
- [18] YADAV S. P., and YADAV S. Image fusion using hybrid methods in multimodality medical images. *Medical and Biological Engineering & Computing*, 2020, 58(4): 669–687. <https://doi.org/10.1007/s11517-020-02136-6>
- [19] DU J., LI W., and TAN H. Three-layer medical image fusion with tensor-based features. *Information Sciences*, 2020, 525: 93–108. <https://doi.org/10.1016/j.ins.2020.03.051>
- [20] WANG Z., CUI Z., and ZHU Y. Multi-modal medical image fusion by Laplacian pyramid and adaptive sparse representation. *Computers in Biology and Medicine*, 2020, 123: 103823. <https://doi.org/10.1016/j.compbiomed.2020.103823>
- [21] MAQSOODS., and JAVED U. Multi-modal Medical Image Fusion based on Two-scale Image Decomposition and Sparse Representation. *Biomedical Signal Processing and Control*, 2020, 57: 101810. <https://doi.org/10.1016/j.bspc.2019.101810>
- [22] CHEN J., ZHANG L., LU L., LI Q., HU M., and YANG X. A novel medical image fusion method based on Rolling Guidance Filtering. *Internet of Things*, 2020, 14: 100172. <https://doi.org/10.1016/j.iot.2020.100172>
- [23] DALAL N., and TRIGGS B. Histograms of oriented gradients for human detection. *Proceedings of the 2005 IEEE*

Computer Society Conference on Computer Vision and Pattern Recognition, 2005, pp. 886–893, <https://doi.org/10.1109/CVPR.2005.177>

[24] WANG D., WAN J., CHEN J., and ZHANG Q. An online dictionary learning-based compressive data gathering algorithm in wireless sensor networks. *Sensors*, 2016, 16(10): 1547. <https://doi.org/10.3390/s16101547>

[25] JANYSHABU S. L., & JAYAKUMAR C. Brain Tumor Classification with MRI Brain Images Using 2-Level GLCM Features and Sparse Representation based Segmentation. Proceedings of the Third International Conference on Intelligent Sustainable Systems, 2020. <https://doi.org/10.1109/ICISS49785.2020.9315971>

[26] REFONAA J., & LAKSHMI M. Accurate Prediction of the Rainfall using Convolutional Neural Network and Parameters Optimization using Improved Particle Swarm Optimization. *Journal of Advanced Research in Dynamical and Control Systems*, 2019, 11(02): 318–328. <https://www.jardcs.org/abstract.php?id=289>

[27] DHAMODARAN S., LAKSHMI M. Ensampling data prediction using sparse data in the mobile intelligent system. *International Journal of Interactive Mobile Technologies*, 2019, 13(10): 106–119. <https://doi.org/10.3991/ijim.v13i10.11311>

[28] VIGNESHWARI S., BHARATHI B., SASIKALA T., and MUKKAMALA S. A study on the application of machine learning algorithms using R. *Journal of Computational and Theoretical Nanoscience*, 2019, 16(8): 3466–3472. <http://dx.doi.org/10.1166/jctn.2019.8309>

[29] EFRON B., HASTIE T., JOHNSTONE I., and TIBSHIRANI R. Least angle regression. *Annals of Statistics*, 2004, 32(2): 407–499. <https://doi.org/10.1214/009053604000000067>

## 参考文献:

[1] JALALI V., & KAUR D. 脑肿瘤检测分类与特征提取技术研究国际多媒体信息检索杂志, 2020, 9(4): 271–290. <https://doi.org/10.1007/s13735-020-00199-7>

[2] SABA T., SAMEH MOHAMED A., EL-AFFENDI M., AMIN J., and SHARIF M. 使用手工和深度学习特征的融合进行脑肿瘤检测。认知的。系统研究, 2020, 59: 221–230, <https://doi.org/10.1016/j.cogsys.2019.09.007>

[3] SHARIF M., AMIN J., RAZA M., ANJUM M. A., AFZAL H., and SHAD S. A. 基于极限学习的脑肿瘤检测。神经计算与应用, 2020, 32(20): 15975–15987. <https://doi.org/10.1007/s00521-019-04679-8>

[4] BAI X., ZHOU F., and XUE B. 利用多尺度中心-环绕礼帽变换通过区域提取融合红外和视觉图像。光学快车, 2011, 19(9): 8444. <https://doi.org/10.1364/oe.19.008444>

[5] AMIN J., SHARIF M., RAZA M., SABA T., SIAL R., and SHAD S. A. 脑肿瘤检测：基于长短期记忆的学习模型。神经计算与应用, 2020, 32(20): 15965–15973. <https://doi.org/10.1007/s00521-019-04650-7>

[6] CHAHAL P. K., PANDEY S., and GOEL S. 磁共振图像脑肿瘤检测技术的调查。多媒体工具 and 应用程序, 2020, 79(29–30): 21771–21814. <https://doi.org/10.1007/s11042-020-08898-3>

[7] SHARIF M., AMIN J., NISAR M. W., ANJUM M. A., MUHAMMAD N., and ALI SHAD S. 一种使用特征融合的基于统一补丁的脑肿瘤检测方法。认知系统研究, 2020, 59: 273–286. <https://doi.org/10.1016/j.cogsys.2019.10.001>

[8] RAJINIKANTH V., RAJ A.N.J., THANARAJ K. P., and NAIK G. R. 一个定制的 VGG19 网络，具有深度和手工特征的串联，用于脑肿瘤检测。应用科学, 2020, 10(10). <https://doi.org/10.3390/app10103429>

[9] WINDISCH P., WEBER P., FÜRWEGER C., EHRET F., KUFELD M., ZWAHLEN D., and MUACEVIC A. 在磁共振成像切片上使用卷积神经网络实现基本脑肿瘤检测的模型可解释性。神经放射学, 2020, 62(11): 1515–1518. <https://doi.org/10.1007/s00234-020-02465-1>

[10] CHANDRAS.K., and BAJPAI M. K. 用于良性脑肿瘤检测和分割的分数曲柄-尼科尔森有限差分法。生物医学信号处理与控制, 2020, 60: 102002. <https://doi.org/10.1016/j.bspc.2020.102002>

[11] SHARIF M., AMIN J., RAZA M., YASMIN M., and SATAPATHY S. C. 融合特征的粒子群优化集成设计用于脑肿瘤检测。模式识别字母, 2020, 129: 150–157. <https://doi.org/10.1016/j.patrec.2019.11.017>

[12] KHAN S. R., SIKANDAR M., ALMOGREN A., UD DIN I., GUERRIERI A., and FORTINO G. 基于医疗物联网的脑肿瘤检测计算方法。下一代计算机系统, 2020, 109: 360–367. <https://doi.org/10.1016/j.future.2020.03.054>

[13] TAN W., TIWARI P., PANDEY H. M., MOREIRA C., and JAISWAL A. K. 大数据时代的多模态医学图像融合算法神经计算与应用, 2020. <https://doi.org/10.1007/s00521-020-05173-2>

[14] HUANG B., YANG F., YIN M., MO X., and ZHONG C. 多模态医学图像融合技术综述。医学中的计算和数学方法, 2020: 8279342. <https://doi.org/10.1155/2020/8279342>

[15] RAJALINGAM B., AL-TURJMAN F., SANTHOSHKUMAR R., and RAJESH M. 具有深度引导滤波的智能多模态医学图像融合。多媒体系统, 2020: 0123456789. <https://doi.org/10.1007/s00530-020-00706-0>

[16] ARIFM., and WANG G. 基于遗传算法的快速曲波变换用于多模态医学图像融合。软计算, 2020, 24(3): 1815–1836 <https://doi.org/10.1007/s00500-019-04011-5>

[17] WANG K., ZHENG M., WEI H., QI G., and LI Y. 使用卷积神经网络和对比金字塔的多模态医学图像融合。传感器, 2020, 20(8): 1–17. <https://doi.org/10.3390/s20082169>

[18] YADAV S. P., and YADAV S. 在多模态医学图像中使用混合方法进行图像融合。医学和生物工程与计算, 2020, 58(4): 669–687. <https://doi.org/10.1007/s11517-020-02136-6>

[19] DU J., LI W., and TAN H. 基于张量特征的多层医学图像融合。信息科学, 2020, 525: 93–108. <https://doi.org/10.1016/j.ins.2020.03.051>

- [20] WANG Z., CUI Z., and ZHU Y. 拉普拉斯金字塔和自适应稀疏表示的多模态医学图像融合。生物学和医学中的计算机, 2020, 123: 103823. <https://doi.org/10.1016/j.combiomed.2020.103823>
- [21] MAQSOODS., and JAVED U. 基于两尺度图像分解和稀疏表示的多模态医学图像融合。生物医学信号处理与控制, 2020, 57: 101810. <https://doi.org/10.1016/j.bspc.2019.101810>
- [22] CHEN J., ZHANG L., LU L., LI Q., HU M., and YANG X. 一种新的基于滚动引导滤波的医学图像融合方法。物联网, 2020, 14: 100172. <https://doi.org/10.1016/j.iot.2020.100172>
- [23] DALAL N., and TRIGGS B. 用于人体检测的定向梯度直方图。2005 年电气和电子工程师学会计算机学会计算机视觉和模式识别会议论文集, 2005, pp. 886–893, <https://doi.org/10.1109/CVPR.2005.177>
- [24] WANG D., WAN J., CHEN J., and ZHANG Q. 无线传感器网络中基于在线词典学习的压缩数据采集算法。传感器, 2016, 16(10): 1547. <https://doi.org/10.3390/s16101547>
- [25] JANYSHABU S. L., & JAYAKUMAR C. 使用 2 级灰度共现矩阵特征和基于稀疏表示的分割的脑肿瘤磁共振成像脑图像分类。第三届智能可持续系统国际会议论文集, 2020. <https://doi.org/10.1109/ICISS49785.2020.9315971>
- [26] REFONAA J., & LAKSHMI M. 使用卷积神经网络准确预测降雨, 使用改进的粒子群优化进行参数优化。动力与控制系统高级研究杂志, 2019, 11(02): 318-328. <https://www.jardcs.org/abstract.php?id=289>
- [27] DHAMODARAN S., LAKSHMI M. 移动智能系统中稀疏数据的采样数据预测. 国际互动移动技术杂志, 2019, 13(10): 106-119. <https://doi.org/10.3991/ijim.v13i10.11311>
- [28] VIGNESHWARI S., BHARATHI B., SASIKALA T., and MUKKAMALA S. 基于 R 的机器学习算法应用研究. 计算与理论纳米科学杂志, 2019, 16(8): 3466-3472. <http://dx.doi.org/10.1166/jctn.2019.8309>
- [29] EFRON B., HASTIE T., JOHNSTONE I., and TIBSHIRANI R. Least angle regression. *Annals of Statistics*, 2004, 32(2): 407–499. <https://doi.org/10.1214/009053604000000067>